Individual variability in sub-Arctic krill material properties, lipid composition, and other scattering model inputs affect acoustic estimates of their population

Brandyn M. Lucca [1], Patrick H. Ressler[2], H. Rodger Harvey [3], and Joseph D. Warren[1]*

[1]School of Marine and Atmospheric Sciences, Stony Brook University, 239 Montauk Highway, Southampton, NY 11968, USA
[2]NOAA, National Marine Fisheries Service, Alaska Fisheries Science Center, 7600 Sand Point Way NE, Seattle, Washington DC 98115, USA
[3]Ocean and Earth Sciences, Old Dominion University, Norfolk, VA 23529, USA

*Corresponding author: e-mail: joe.warren@stonybook.edu.

Target strength model inputs including morphometry, material properties, lipid composition, and *in situ* orientations were measured for sub-Arctic krill (*Euphausia pacifica*, *Thysanoessa spinifera*, *T. inermis*, and *T. raschii*) in the eastern Bering Sea (EBS, 2016) and Gulf of Alaska (GOA, 2017). Inter-species and -regional animal lengths were significantly different ($F_{1,680} = 114.10$, $p < 0.01$), while animal shape was consistent for all species measured. The polar lipid phosphatidycholine was the dominant lipid, comprising $86 \pm 16\%$ (mean $\pm$ SD) and $56 \pm 22\%$ of total lipid mass in GOA and EBS krill, respectively. Krill density contrasts varied by species and region rather than with morphometry, lipid composition, or local chl$_a$ fluorescence. Mean *in situ* krill orientation was $1 \pm 31°$, with 25% of observed krill within $\pm 5°$ of broadside incidence. Modelled target strength sensitivity was frequency independent for variations in material properties but was primarily sensitive to morphometry and orientation at lower (38 kHz) and higher (200 kHz) frequencies, respectively. Measured variability in material properties corresponded to an order of magnitude difference in acoustic estimates of biomass at 120 kHz. These results provide important inputs and constraints for acoustic scattering models of ecologically important sub-Arctic krill species.

Keywords: acoustics, Bering Sea, Gulf of Alaska, krill, material properties, target strength

Introduction

Euphausiids (i.e. krill) are a keystone species in the Gulf of Alaska (GOA) and eastern Bering Sea (EBS) ecosystems, supporting commercially important fishes such as walleye pollock (*Gadus chalcogrammus*; Buckley *et al.*, 2016), Pacific cod (*Gadus macrocephalus*; Farley et al., 2016), and both marine mammals and seabirds (Aydin and Mueter, 2007; Hunt *et al.*, 2016). Traditionally krill (primarily *Thysaneossa* spp.) in these ecosystems are surveyed via net trawls (Hunt *et al.*, 2016), yet these capture methods are likely to underestimate krill densities (Sameoto *et al.*, 1993; Wiebe *et al.*, 2013) due to net avoidance (Sameoto *et al.*, 2000), mesh size and subsequent escapement, spatially patchy distribution of aggregations (Mauchline, 1980), and diel variability (Simard and Sourisseau, 2009). Active acoustic surveys provide an attractive alternative sampling method with fine-scale information on krill abundance and distribution over large geographic areas and extended time periods (Simmonds and Maclennan, 2005; Reiss *et al.*, 2008), but are known to over- or underestimate krill abundance relative to net sampling (Warren and Wiebe, 2008) and be subject to the inherent uncertainty in the acoustic properties of the animals (Hunt *et al.*, 2016).

Spatiotemporal distributions of EBS and GOA krill abundance and biomass are currently measured using acoustic trawl surveys (Honkalehto *et al.*, 2009; Ressler *et al.*, 2012) and stereo camera

deployments (Levine *et al.*, 2018). Target strength (TS, dB re 1 m^2), which represents the acoustic backscattering cross-section of an individual organism, a necessary variable for converting acoustic backscatter measurements into estimates of animal numerical density, and indirectly abundance and biomass (Simmonds and Maclennan, 2005). TS is a function of the transmitted acoustic frequency, ambient sound speed of seawater, body morphology, behaviour (e.g. orientation in the water column, body curvature, flexure), and material properties (Stanton *et al.*, 1998; Stanton and Chu, 2000; Lawson *et al.*, 2006). Krill TS can be estimated using theoretical scattering models, such as distorted wave Born approximation (DWBA) and other variants (Chu *et al.*, 1993; Stanton *et al.*, 1998, Demer and Conti, 2003; Jones *et al.*, 2009), and *in situ* backscatter measurements (Lawson *et al.*, 2006). Appropriate model parameterization will improve both the precision and accuracy of krill multifrequency classification (Holliday, 1977; Ressler *et al.*, 2012) and abundance/biomass estimates (Simmonds and Maclennan, 2005).

The majority of krill TS models rely on parameter inputs that include (i) measurements of different species reported in the literature (e.g. Foote, 1990; McQuinn *et al.*, 2013; Jech *et al.*, 2017), (ii) empirical, laboratory measurements collected from refrigerated samples (Greenlaw and Johnson, 1982; Køgeler *et al.*, 1987); or (iii) shipboard measurements (Chu and Wiebe, 2005; Smith *et al.*, 2010; Sakinan *et al.*, 2019) from (in some cases) live animals. Previous surveys measured many of these parameters for northeastern Pacific (Becker and Warren, 2014) and sub-Arctic krill (Smith *et al.*, 2010), with the latter used to parameterize and produce a theoretical TS model for EBS krill (Ressler *et al.*, 2012; Smith *et al.*, 2013). Modelled TS for EBS krill were sensitive to observed variability in parameter inputs (Ressler *et al.*, 2012; Smith *et al.*, 2013). For example, the assumed difference in broadside and perpendicular (relative to the sea surface) *in situ* orientations of krill can shift theoretical TS as much as 40 dB at frequencies in the geometric scattering region (McGehee *et al.*, 1998; Smith *et al.*, 2013); some models may thus be overly sensitive to changes in orientation thereby underestimating TS (Demer and Conti, 2003). Similarly, small variations in material properties ($\sim$2–4%) can yield substantial changes in theoretical TS at certain frequencies (e.g. up to 20 dB, Stanton and Chu, 2000). Consequently, the uncertainty in different parameter estimates and how each propagates to differences in TS model outputs needs to be better understood.

Changes in food availability and possible differences in animal lipid content has been hypothesized as an explanation for previous observations of spatial variability in EBS krill material properties (Smith *et al.*, 2010). Recent analyses of krill lipid composition show a possible relationship between lipid composition and energy storage for *T. raschii* (Pleuthner *et al.*, 2016). The complex lipid distribution observed within krill is likely a function of nutrition, reproductive stage, and feeding history. Seasonal inter- and intra-species differences in lipids among North Atlantic sub-Arctic krill (Cabrol *et al.*, 2019) may explain some of the spatiotemporal signals observed in material properties for other krill (McQuinn *et al.*, 2013). Furthermore, the heterogeneous distribution of lipids throughout the body suggest that the standard model assumption of homogeneity in material properties requires validation (Jech *et al.*, 2015). Despite these potential considerations, the relationship between material properties, lipid amount and type, and acoustic scattering has not been well-studied for crustaceans (Yayanos *et al.*, 1978;

Knutsen *et al.*, 2001). An exception is Sakinan *et al.* (2019) who recently incorporated lipid content into a TS model for the copepod *Calanus finmarchicus*.

This study measured species- and location-specific material properties, morphometry, lipid composition and *in situ* behaviours of live, or recently expired, krill. The effect of observed parameter variability on modelled TS was also evaluated using simulations at standard scientific echosounder frequencies (i.e. 38, 70, 120, and 200 kHz). We conclude by considering sources of uncertainty and providing suggestions for future applications of this parameterized TS model, including suggested parameter distributions that are relevant for surveys of EBS and GOA krill stocks as well as those in other ecosystems.

Methods

Overall survey design

Sampling and shipboard experiments were conducted aboard the NOAA Ship *Oscar Dyson* during portions of pollock acoustic trawl surveys in the EBS (13 June–03 July 2016; Honkalehto *et al.*, 2018) and GOA (30 July–16 August 2017; Jones *et al.*, 2019). Krill were captured in near-surface day- and night-time Methot trawls (max depth = 278 m, mean depth = 124 ± 51 m) with a 5 m^2 mouth area, 3 × 2 mm mesh in the body, and 1 mm mesh in the codend (Methot, 1986) from 31 stations (Figure 1). Daily conductivity-temperature-depth (CTD) vertical profiles were conducted to collect environmental data and the closest measurements in time were assigned to each Methot tow. The catch was washed from the codend of the trawl into a large tub for sorting. A sub-sample from each trawl catch of at least 25 living krill was selected for further morphometric (i.e. shape, length, mass), taxonomic (i.e. species), and material property measurements. Live krill were maintained in multiple small (4 l), aerated aquaria in a temperature controlled (2–4°C) environment if they were not processed immediately. Stereo camera deployments occurred at 24 stations that were used to estimate *in situ* orientation of krill (Levine *et al.*, 2018). All statistical comparisons were made using R 4.0.1 (R Core Team, 2020) and related visualization and support packages (Fox and Weisberg, 2019; Wickham *et al.*, 2019). General statistical comparisons were made using Type-II ANOVAs and Welch's *t*-test (α = 0.05).
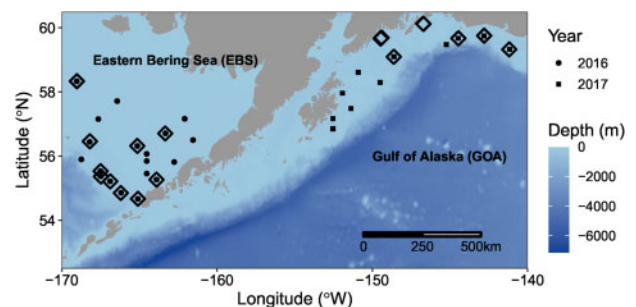

Figure 1. Krill were collected from 19 EBS (dots) and 11 GOA (squares) unique sites via Methot tows. Stereo camera deployments (hollow diamonds) occurred at 11 EBS and 13 GOA stations, although some casts were done near one another. Bathymetric data were imported from NOAA (Amante and Eakins, 2009) using the *marmap* R-package (Pante and Simon-Bouhet, 2013).

Animal morphometry

All animals were digitally photographed to measure animal shape and size. Individual krill were laid out on sorting trays as straight as possible to capture lateral (left side of animal) images. These specimens were then photographed (with an Olympus TG-3 digital camera using the built-in macro mode, *f*: 5.5–18.0 mm, shooting range: 0.01–0.10 m) with a reference scale included in the image. Animals were then rearranged on the tray to capture the dorsal (top-down) view. The images were processed using a custom MATLAB (R2018a, v. 9.4) program where the user generated an along-body line by clicking on the anterior of the eye and posterior of the sixth abdominal segment, which represents Standard Length 2 (SL2, mm; Mauchline, 1980) that is commonly used in TS modelling (Lawson *et al.*, 2006). Perpendicular lines at 16 equidistant points were then generated; the user selected the intersection of these lines and the body to capture the height/width of the animal by converting the number of pixels to mm using the reference ruler as a calibration (Figure 2). Shapes were then normalized by dividing SL2 of each animal from their respective along-body (0 to 1) and height (−1 to 1) axes. SL1 length (anterior of the eye stalk to the posterior end of the telson and uropods; Mauchline, 1980) was also measured to produce an SL2–SL1 linear regression and for other comparisons with literature values. Lastly, a linear regression was used to assess the log-linear relationship between SL2 and mass (mg).

Material properties

Animals were anesthetized using sodium bicarbonate tablets or recently (<20 min) expired prior to any material property measurements being made. Animal density (ρ_animal, g ml^{-1}) was measured using the titration method (Warren and Smith, 2007) where a high-density solution was created using measured volumes of glycerin ($\rho = 1.173$ g ml^{-1}) and seawater in a temperature-controlled room at 2–4°C. Salinity of the seawater was recorded before measurements were conducted. This solution was then added to a beaker containing one or more animals and a

Figure 2. Animal shapes were measured from individual krill at 16 equidistant points along the animal's body. The red line represents a 1 mm calibration line, the yellow dots and orange lines represent the two-dimensional equidistant points used to approximate the discretized cylinders that parameterize TS models, and the yellow line represents the overall lateral two-dimensional shape of the animal.

known volume of ambient seawater. Once the animal became neutrally buoyant, the volumes of both fluids in the beaker and the temperature of the beaker solution were recorded. Seawater density (ρ_sw) was calculated using the *marelac* package in R (Soetart and Petzoldt, 2018) to estimate the density contrast ($g = \rho_\text{animal}/\rho_\text{sw}$) of krill ($n = 272$ and 325 in 2016 and 2017, respectively).

The time–travel difference method (Chu and Wiebe, 2005; Smith *et al.*, 2010) was used to estimate the bulk sound speed contrast (*h*) of captured krill samples. Measurements ($n = 250$ pings) were made in a 77 ml polyvinyl chloride (PVC) t-tube with two 192 kHz bronze single-beam, narrowband transducers (Lowrance TH-NB), clamped at each end to create a water-tight seal. A signal generator (Beckman Industrial), wideband power amplifier (Krohn-hite 7500), and digitizing oscilloscope (Picotech 5000 series) were used to generate a continuous wave at 192 kHz with a peak-to-peak amplitude of 2 V and pulse duration of 5 µs. The salinity and temperature of ambient seawater collected from the ship's flow-through seawater system were measured at the start and end of the measurements (c_sw, Soetaert and Petzoldt, 2018). Krill were rinsed, sieved, and gently patted with a paper towel to reduce any excess water content. These organisms were then placed into the t-tube; seawater was added to fill the remaining t-tube volume. All waveforms were processed using the SciPy library (Jones *et al.*, 2001) in Python 3.7.1 (Python Software Foundation, 2018). A band-pass filter was applied to remove transient and impulsive noise. A peak detector was then used to determine the time-of-arrival for the transmitted waveform for both the empty and animal-filled measurements.

Does lipid composition vary with species and location?

After krill material property were completed, individual animals were placed in 5 and 7 ml cryovials and frozen at −80°C. Samples were kept frozen during transportation to a shore-based laboratory for lipid analysis. Both wet and dry weights of previously frozen krill were measured and animals lyophilized prior to lipid extraction. Total lipid extraction (TLE) was conducted using microwave-assisted solvent extraction (2:1 DCM: MeOH MARS five system) following the methods described by Harvey *et al.* (2012). Once extracted, intact lipid class structural analysis was conducted using Reverse Phase Liquid Chromatography-Mass Spectrometry (RP LC-MS). Lipid extracts were separated using an Agilent 1290 ultra-high performance liquid chromatography system (C18 Eclipse Column) with structural identification via LTQ XL Orbitrap Mass Spectrometer (Thermo Scientific) LC-MS methods described by Bird *et al.* (2011) were followed with some modifications made to the mass spectrometry protocol to accommodate different instrumentation and calibration. Separated lipids initially entered the Fourier-transform Mass Spectrometer (Orbitrap) and were detected in profile mode (60 000 scan rate in Normal mode). Subsequent collision-induced dissociation fragmentation (to MS^2 or MS^3) took place in the Ion Trap Mass Spectrometer with data collection in centroid mode. Dynamic exclusion was employed at a frequency of 30 s with decreasing amounts of time as the fragmentation progressed from MS^2 to MS^3. All samples were run in both positive and negative electrospray ionization modes in order to best detect the range of lipid classes that could be present. To determine if the acoustic experimental measurements performed on krill caused changes in their lipid content, lipids were also measured for a control group

of "pristine" krill, which were frozen immediately after being sorted from the net haul.

Does lipid content, fluorescence, or length affect krill density?

Food availability (i.e. phytoplankton) was characterized by using chl$_a$ fluorescence (mg m^{-3}) as a proxy (Kolber and Falkowski, 1993), which was measured by a Wet Labs ECO-AFL/FL fluorometer from each CTD profile to investigate the potential relationship between g and feeding status (Smith *et al.*, 2010). Fluorescence measurements were averaged in 1 m vertical bins and four different metrics were calculated: maximum fluorescence (F_{max}), integrated fluorescence over entire water column (F_{int}), fluorescence measured at the mixed layer depth (F_{mld}), and integrated fluorescence from the surface to the mixed layer depth (F_{mldint}).

A linear mixed model (Bates *et al.*, 2015) was used to assess the effects on g of TLE, length, fluorescence, mass, species, region, and body condition. Species, region, and condition were treated as random effects. Since the four species were not all present within each region, species was nested by region. Similarly, TLE was grouped by body condition. Mass, length, fluorescence, TLE, and all interactions were treated as fixed effects. Since there were substantially different sample sizes for paired measurements of g, TLE, length, mass, and fluorescence, four models were assessed: (i) lipid ($g \sim$ TLE, length, mass, fluorescence), (ii) mass-fluorescence-length ($g \sim$ length, mass, fluorescence), (iii) fluorescence-length ($g \sim$ length, fluorescence), and (iv) length ($g \sim$ length). Separate iterations of each model were also run using each of the four different fluorescence metrics and were compared using the root-mean square error (RMSE) for each model. The goodness-of-fit for each model was assessed using marginal R^2 for fixed effects (or R_M^2) and the total conditional R^2 (or R_C^2) with random effects included (Nakagawa and Schielzeth, 2013).

How does *in situ* orientation of krill vary?

In situ estimates of orientation (relative to the surface) of individual krill in the water column were measured using two stereo camera systems and Sebastes Image Analysis software (Williams *et al.*, 2016; Levine *et al.*, 2018). There are different frames of reference to describe the orientation of an acoustic target. Stereo camera measurements of krill orientation, θ_{animal}, use the tilt of an animal's body relative to the sea surface, where $-\pi/2$ and $\pi/2$ represent the anterior (head) and posterior (telson) of the krill facing exactly away from (i.e. head-down) and towards (i.e. head-up) a theoretical hull-mounted transducer, respectively. Once the camera was deployed to depth, the orientations of the first 100 unique animals were recorded. This process was completed for each of the 27 camera deployments. Orientation measurements were corrected for the roll and pitch of the camera following the procedures outlined in Levine *et al.* (2018).

Although orientations are typically reported as normal distributions in the literature (Kils, 1981; Lawson *et al.*, 2006; Kubilius et al., 2015; Levine *et al.*, 2018), the underlying data are bounded by $[-\pi/2, \pi/2]$ and therefore must be handled differently to appropriately deal with values that approach the distribution's boundaries (Landler *et al.*, 2018). Therefore, the von Mises distribution, f_{vM} ($\theta_{animal} \in ([-\pi/2, \pi/2] \mid \mu, \kappa)$ or equivalent f_{vM} ($\theta_{animal} \in ([-90°, 90°] \mid \mu, \kappa)$, was used to describe *in situ* krill orientation, which is an approximation of the wrapped normal distribution, f_{WN} ($\theta_{animal} \in ([-\pi/2, \pi/2] \mid \mu, \sigma)$, which has been used for Antarctic krill TS modelling (e.g. Bestley *et al.*, 2017). The von Mises distribution comprises two parameters that represent the measure of location (μ) and concentration (κ) and approaches a normal distribution, $N(\mu = \mu, \sigma^2 = \kappa^{-1})$, whereby as κ approaches infinity. Mean and *SD* values describing orientation were evaluated using the *circular* R-package (Agostinelli and Lund, 2017). A two-sample Kolmogorov–Smirnov (KS) test was then used to compare differences in the distribution of daytime and night-time camera deployments.

How sensitive are TS models to measured variability of parameter inputs?

The DWBA model (Chu *et al.*, 1993) for a deformed cylinder was used to assess the sensitivity of TS to measured distributions for each parameter. This model integrates the acoustic backscatter over the volume of the animal, which is broken up into N ($n = 15$) number of discrete cylindrical disks:

$$f_{bs_j}(\theta_{model}) = \frac{k_1}{4} \int (Y_k - Y_\rho) \, e^{-2ik_2\vec{r_0}} a_j \, \frac{J_1(2k_2 a_j \cos\beta_{tilt})}{\cos\beta_{tilt}} \, d\vec{r_0} \quad (1)$$

$$f_{bs}(\theta_{model}) = \sum_{j=1}^{N} f_{bs_j}(\theta_{model}), \quad (2)$$

where θ_{model} ($\theta_{model} = \theta_{animal} + \pi/2$) is the orientation of the incident soundwave relative to the target's body, where $\pi/2$ and $3\pi/2$ radians are considered to be broadside, i is the imaginary unit ($\sqrt{-1}$), J_1 is the Bessel function of the first kind of order 1, k_1, and k_2 represent the acoustic wavenumber in the ambient seawater and the animal's body, respectively, a_j is the radius of the jth cylindrical disk along the body, β_{tilt} is the tilt angle of the jth cylindrical disk, and r_0 is the position matrix that represents the x, y, and z coordinates of the animal shape (m). The material property parameter (M, Smith *et al.*, 2010) represents $|\gamma_\kappa - \gamma_\rho|$, where

$$M = |Y_k - Y_\rho| = \left| \frac{1}{gh^2} + \frac{1}{g-2} \right|. \quad (3)$$

This is then converted to TS via:

$$TS = 20\log_{10}\left(|f_{bs}(\theta_{model})|\right). \quad (4)$$

Combined uncertainty in f_{bs} (which is analogous to σ_{bs}) given variability in parameter measurements was estimated using Monte Carlo methods by randomly drawing model input values from normal distributions ($n = 10\,000$) of maximum carapace radius, θ_{model}, and M. These inputs parameterized the DWBA [Equations (1) and (2)] at standard scientific echosounder frequencies (i.e. 38, 70, 120, and 200 kHz) using a mean animal shape (non-curved). Coefficients of variation of the mean [CV_{SE}: standard error (s.e.) of f_{bs} divided by mean f_{bs}, sometimes known as the relative s.e.] were calculated to estimate how the combined uncertainty from parameter inputs propagated into the precision of estimates of mean f_{bs}. Mean CV_{SE} and the s.e. of the mean were also calculated to test the effect of sample size (i.e. $n = 100$

and 1000) by resampling (without replacement) from the original 10 000 samples for a total of 1000 bootstrapped replicates. The more standard coefficient of variation (*CV*: *SD* of f_{bs} divided by mean f_{bs}) was also estimated to assess how the variability in parameter distributions affected the relative dispersion and uncertainty of modelled f_{bs}. Models were generated using the acoustic TS R-package (Lucca, 2020).

A local sensitivity analysis was performed to estimate gradients in f_{bs} with respect to small perturbations in radius, length, θ_{model}, and M (i.e. *g* and *h*). Gradients were calculated using Forward Mode Automatic Differentiation that decomposes a function into a series of differentiable operations (e.g. "+") and calculates the partial derivative with respect to each parameter that are then summed via the chain rule (Baydin *et al.*, 2018). The algorithm was initialized using mean parameter values. In order to directly compare local sensitivity to each parameter, gradients were scaled to dimensionless values to represent the relative sensitivity (RS), sometimes referred to as "elasticity" or "proportional sensitivity" in the literature:

$$RS = \frac{\partial f_{bs}}{\partial X} \frac{X_1}{f_{bs_1}}, \qquad (5)$$

where $\partial f_{bs}/\partial X$ is the change in f_{bs} with respect to the parameter vector *X*, X_1 is the vector of mean parameter values, and f_{bs1} is modelled f_{bs} given X_1. This metric represents the proportional change in f_{bs} given a 1% increase in each parameter. Both the ForwardDiff Julia (Revels *et al.*, 2016) and JuliaCall R (Li, 2019) packages were used for this analysis. The relative influence of shape was evaluated by calculating gradients using individual body shapes of all krill, which were then resampled with replacement (*n* = 1000) to construct bootstrapped 80% *CI*s. A tapered cylinder from previous EBS measurements (Smith *et al.*, 2013) and a generic krill shape (McGehee *et al.*, 1998) were also included for additional comparisons. Lastly, TS at 120 kHz and biomass estimates generated using this study's *M* distribution were compared to hypothetical calculations from other material property measurements in the literature. Normal and uniform

distributions of *g* and *h* (*n* = 10 000) were simulated depending on whether a mean ± *SD* or minimum and maximum were reported, respectively.

Due to the relative complexity of how sound scatters, the position and magnitude of theoretical nulls at higher frequencies may not represent realistic backscatter from an individual target. These frequencies, which are typically in the geometric scattering region, are especially sensitive to changes in orientation, thereby possibly artificially skewing TS distributions. A stochastic phase variability term, φ (radians), was included in the model to mitigate these uncertainties to produce a stochastic DWBA (SDWBA; Demer and Conti, 2003) that is a variation of Equation (2). This SDWBA was run in parallel to investigate how reducing the effects of off-broadside incidence influences simulated TS:

$$f_{bs}(\theta_{model}) = \sum_{j=1}^{N} f_{bs_j}(\theta_{model})e^{i\varphi_j}, \qquad (6)$$

where φ_j is drawn from the normal distribution $N(0, \sigma_\varphi)$ (Demer and Conti, 2003). Both σ_φ and the number of body cylinders were adjusted with increasing frequencies to account for the change in ratio between spatial resolution and wavelength (Conti and Demer, 2006). Consequently, reference krill parameters (L_0 = 17.9 mm, *N* = 15 cylinders, f_0 = 120 kHz) corresponded to $\sigma_{\varphi 0}$ = 0.31 when compared against the σ_φ = 0.71 reported by Conti and Demer (2006) for a 38.35 mm krill with 14 cylinders at 120 kHz. Although the number of cylinders increased with frequency (*N* = 15–47), *N* = 15 was set as the minimum regardless of frequency.

Results
Animal morphometry
Species used for this analysis differed between the EBS (*T. inermis*, *T. raschii*, and *T. spinifera*) and GOA (*T. inermis*, *T. spinifera*, and *E. pacifica*) habitats. GOA krill (18.9 ± 4.1 mm, *n* = 413) were significantly larger than in the EBS (16.7 ± 2.3 mm, *n* = 273; $t_{667.4}$ = −8.99, *p* < 0.01, Figure 3). Mean length also significantly
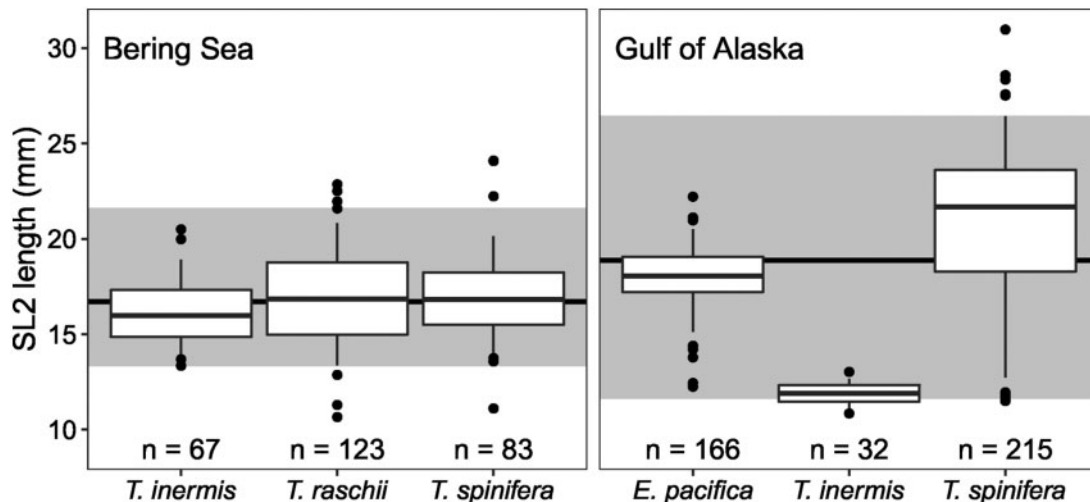

Figure 3. Krill SL2 length (mm) varied within and among species between the 2016 EBS (left) and 2017 GOA (right) field seasons. EBS krill showed similar length estimates while there was high variability among GOA krill species. The extent of each box and whisker represents the interquartile range and the 95th percentile confidence interval, respectively. The horizontal black line represents the mean length for each region. The shaded area represents the 95th percentile confidence interval of length for each region.

differed among krill species both between ($F_{1,681}$ = 88.9, $p < 0.01$) and within ($F_{1,680}$ = 114.10, $p < 0.01$) geographic regions. Post hoc pairwise comparisons indicated that mean length of *T. spinifera* (19.6 ± 4.2, $n = 298$), *E. pacifica* (18.0 ± 1.6 mm, $n = 166$), *T. inermis* (14.8 ± 2.4, $n = 99$), and *T. raschii* (16.9 ± 2.5, $n = 123$) were all significantly different. Among GOA krill, mean length was significantly greater ($p < 0.05$) for *T. spinifera* (20.6 ± 4.3 mm, $n = 215$) than *T. inermis* (11.9 ± 0.6 mm, $n = 32$) and *E. pacifica*. Conversely, there were no significant differences in mean length among any of the EBS krill species. When comparing differences between each region, GOA *T. spinifera* and EBS *T. inermis* (16.1 ± 1.6 mm, $n = 67$) were significantly larger than EBS *T. spinifera* (17.0 ± 2.3 mm, $n = 83$) and GOA *T. inermis*, respectively.

When normalized to the length of each animal, inter-species shape was consistent with the highest amount of variability observed around the carapace (i.e. 0.0 to ~0.1 normalized length or up to 10% of maximum length, Figure 4). The linear relationship between SL1 and SL2 varied among species and between regions

(Table 1) but were comparable to the relationship reported by Lawson *et al.* (2006) and primarily represent the telson length. There was also a significant positive linear relationship between SL2 and mass for all species, although only GOA *T. spinifera* was relatively strong ($R^2_{adj} = 0.74$).

Material properties

Mean GOA density contrast (1.021 ± 0.006, $n = 263$) was significantly greater than in EBS krill (1.018 ± 0.006, $n = 272$; $t_{525.3} = -6.96$, $p < 0.01$). Significant differences among species ($F_{3,529} = 14.9$, $p < 0.01$) and the interaction of species and regions ($F_{1,529} = 77.7$, $p < 0.01$) demonstrated relatively large variability in distributions of both inter- and intra-species g (Figure 5). Specifically, pairwise differences in mean g measured for *E. pacifica* (1.023 ± 0.005, $n = 104$), *T. inermis* (1.017 ± 0.006, $n = 100$), *T. raschii* (1.018 ± 0.005, $n = 123$), and *T. spinifera* (1.020 ± 0.006, $n = 208$) were all statistically significant. Within GOA, *E. pacifica* were denser than *T. spinifera* (1.019 ± 0.006, $n = 126$; $p < 0.01$), but not *T. inermis* (1.023 ± 0.005, $n = 33$;
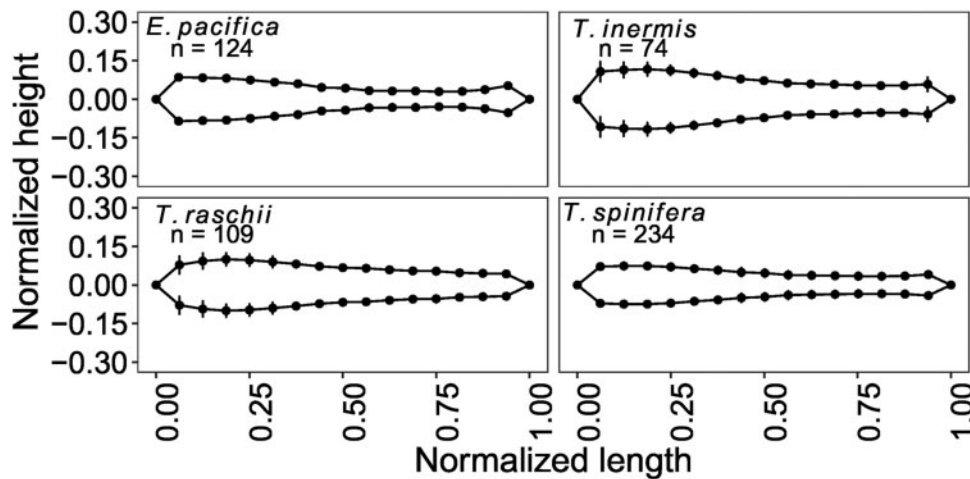

Figure 4. Normalized animal shapes extracted from photographs of the lateral views from the four captured krill species (*Thysanoessa inermis, T. raschii, T. spinifera,* and *Euphausia pacifica*) showed similar variability in body shape. Animal lengths were scaled to a [0, 1] distribution. Heights were scaled to the maximum length of each animal and centred around $y = 0$. Vertical bars represent mean scaled height ± 1 SD.

Table 1. Regression relationships between SL2 and SL1 length (mm; SL2 = β_{SL1}(SL1) + β_0 + ε) and SL2 length and mass (mg; $\log_{10}$(Mass) = $\log_{10}(\beta_0)$ + $\beta_{SL2}\log_{10}$(SL2) + ε) showed both inter- and intraspecies differences.

Species	Region	SL2 = β_{SL1} (SL1) + β_0 + ε				$\log_{10}$(Mass) = $\log_{10}(\beta_0)$ + $\beta_{SL2}\log_{10}$(SL2) + ε				
		β_{SL1}	β_0	R^2_{adj}	n	β_{SL2}	β_0	R^2_{adj}	n	σ_{corr}
Euphausia pacifica	GOA	0.84 ± 0.02	−0.18 ± 0.02	0.95	166	3.07 ± 0.54	−2.16 ± 0.67	0.28	83	1.05
Thysanoessa inermis	GOA	0.82 ± 0.05	0.50 ± 0.05	0.89	32	N/A	N/A	N/A	2	N/A
T. inermis	EBS	0.78 ± 0.03	1.38 ± 0.04	0.89	67	3.22 ± 1.94	−2.33 ± 2.34	0.07	23	1.16
T. spinifera	GOA	0.85 ± 0.01	−0.24 ± 0.01	0.99	215	3.49 ± 0.21	−2.52 ± 0.28	0.74	96	1.06
T. spinifera	EBS	0.85 ± 0.03	−0.24 ± 0.01	0.93	83	3.12 ± 1.16	−2.14 ± 1.40	0.26	19	1.04
T. raschii	EBS	0.82 ± 0.02	0.45 ± 0.02	0.95	123	2.69 ± 0.75	−1.70 ± 0.75	0.24	38	1.10
All species	GOA	0.85 ± 0.01	0.51 ± 0.27	0.99	413	3.67 ± 0.19	−2.83 ± 0.25	0.23	181	1.07
	EBS	0.82 ± 0.01	−0.20 ± 0.10	0.93	273	2.91 ± 0.63	−1.95 ± 0.75	0.28	80	1.10
All species		0.84 ± 0.01	0.07 ± 0.10	0.98	686	3.65 ± 0.18	−2.81 ± 0.22	0.61	261	1.07

Estimates of β_{SL1} and β_{SL2} represent the slope coefficients (± s.e.), β_0 represents the intercept coefficient, R^2_{adj} represents the adjusted R^2 goodness-of-fit, n is the sample size, and σ_{corr} is the correction factor that accounts for back-transformation bias when predicting linear mass via $10^{5 \times \sigma(residual)}$, where σ(residual) represents the model residual variance.
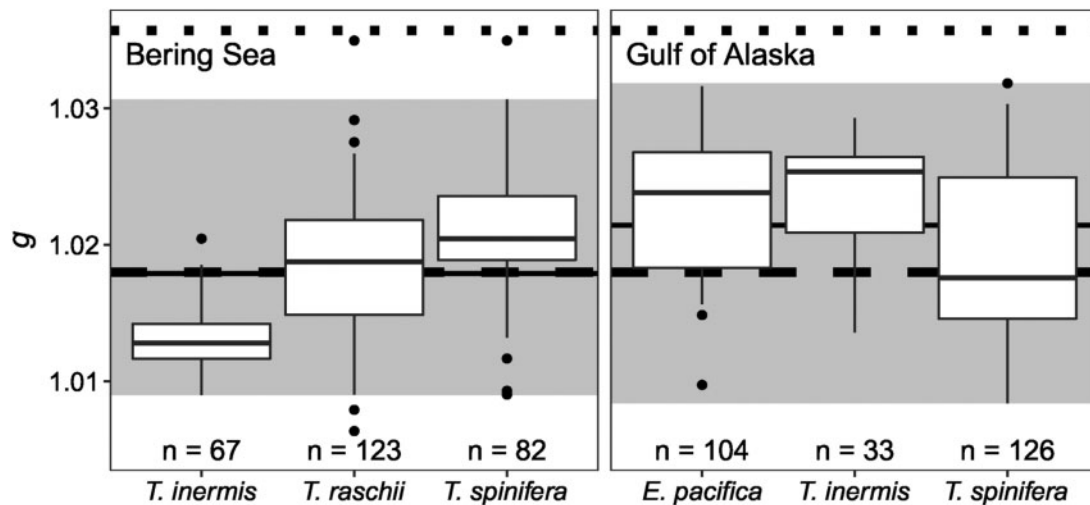
Figure 5. Animal density contrast (*g*) varied within and among species of krill between the 2016 EBS (left) and 2017 GOA (right) field seasons. Animals with higher estimates of *g* would produce larger TS estimates, assuming all other variables were held constant. Mean *g* in both regions (solid black line) were more similar to previously reported values in the EBS for sub-Arctic krill (black-grey dashed line, principally *Thysanoessa* spp., Smith *et al.,* 2010) than values for Antarctic krill (black dotted line, *Euphausia superba,* Foote, 1990). The extent of each box and whisker represents the interquartile range and the 95th percentile confidence interval, respectively. The shaded area represents the 95th percentile confidence interval of *g* for each region.

$p = 0.99$). GOA *T. inermis* were significantly denser than their EBS counterparts (1.013 ± 0.003, $n = 67$; $p < 0.01$), while EBS *T. spinifera* (1.021 ± 0.005, $n = 82$) were denser than GOA *T. spinifera* ($p < 0.01$). GOA *h*-measurements were significantly greater and less variable (1.037 ± 0.011 $n = 23$) than in the EBS (1.022 ± 0.018, $n = 13$; $t_{17.09} = -2.75$, $p = 0.01$). Overall, the mean *h* for all measurements made in this study was 1.032 ± 0.015 ($n = 36$). Both the region-specific and overall distributions of *h* were dissimilar from what was previously reported in the EBS (1.005 ± 0.008, Smith *et al.,* 2010).

Does lipid composition vary with species and location?
Intact phospholipids were the major lipid class observed across all animals with phosphatidylcholine (PC) comprising up to 97% (by mass) of total lipids of individuals with an overall mean of 71 $\pm$ 25% (Figure 6). PC was highest for all four species with means of 95 $\pm$ 2%, 72 $\pm$ 20%, 53 $\pm$ 17%, and 51% $\pm$ 24% in *E. pacifica*, *T. spinifera*, *T. inermis*, and *T. raschii*, respectively. There was a strong regional difference in lipid composition where PC comprised mean of 86 $\pm$ 16% and 56 $\pm$ 22% in GOA and EBS krill, respectively. Unlike GOA krill, EBS krill contained also had large contributions from triglycerols (TAG) (27 $\pm$ 19%) and lysophosphatidylcholine (LPC) (6 $\pm$ 8%). Aside from *E. pacifica*, TAG made up the second largest proportion of lipids for GOA *T. spinifera* (9 $\pm$ 8%), EBS *T. spinifera* (17 $\pm$ 18%), EBS *T. inermis* (32 $\pm$ 16%), and EBS *T. raschii* (28 $\pm$ 21%).

Lipid composition appeared to be somewhat sensitive to manipulations caused by the acoustic experiments (Figure 7). Pristine krill ($n = 10$; *T. inermis* $n = 6$, *T. raschii* $n = 4$) had approximately equal mean proportions of TAG (45 $\pm$ 8%) and PC (44 $\pm$ 9%), which differed from their manipulated counterparts (TAG = 23 $\pm$ 18%, PC = 67 $\pm$ 18%). Mean total lipid in pristine animals (49.2 $\pm$ 26.8 mg g^{-1}, $n = 10$) was also greater than in manipulated animals (25.2 $\pm$ 20.4 mg g^{-1}, $n = 18$; $W = 32$, $p < 0.01$). One caveat to these observed differences is that pristine krill were not routinely collected throughout the cruises,

and pristine krill analysed originated from a single tow separate from manipulated krill of the same species.

Does lipid content, fluorescence, or length affect krill density?
Krill density contrasts were not significantly affected by lipid content or fluorescence. Aside from the lipid model where F_{int} improved the relative goodness-of-fit (RMSE = 0.0040, 0.0043, 0.0043, and 0.0045 for F_{int}, F_{mldint}, F_{mld}, and F_{max}, respectively), all of the fluorescence metrics yielded near-identical performances. Density contrast decreased with increasing length ($n = 520$) but was otherwise independent of TLE ($n = 24$), mass ($n = 124$), and fluorescence ($n = 313$). The linear relationship between *g* and length was very weak across all models ($\beta_{length} = -7.9E-4$ to $-4.8E-4$) including the length-specific model [$-6.7E-4$ ($-8.1E-4$, $-5.2E-4$), $\beta_0 = 1.030$ (1.026, 1.034), $R^2_M = 0.11$, $R^2_C = 0.50$]. Overall, both species and region explained more of the variation observed in *g* ($R^2_C = 0.50$–0.59) than the fixed effects ($R^2_M = 0.11$–0.16) across all models.

How does in situ orientation of krill vary?
Mean *in situ* krill orientation, θ_{animal}, was 1 $\pm$ 31° (directional mean $\pm$ circular *SD*, $n = 2,700$; Figure 8), with 25% of observed krill within $\pm$5° of broadside incidence. Comparatively, θ_{animal} was 2 $\pm$ 31° using the mean and *SD* when not assuming a wrapped distribution (i.e. f_{vM}). There was a significant difference in distribution of orientations between day- and night-time camera trawls (two-sample KS test, $D = 0.144$, $p < 0.01$). Day-time orientations were significantly more positive (i.e. head-up: 5 $\pm$ 39°, $n = 400$) than at night (i.e. broadside: 0 $\pm$ 28, $n = 2300$; KS test, $D = 0.106$, $p = 0.02$). These observed means were similar to the near-horizontal *in situ* orientations of ~10° (Hamner *et al.,* 1983), -9.8 ± 34.1° (Kristensen and Dalen, 1986), 9.7 $\pm$ 59.3° (or 0.0 $\pm$ 27.3° when removing krill beyond $\pm$ 100°; Lawson *et al.,* 2006), -9 ± 14 to 17 $\pm$ 37° (Kubilius *et al.,* 2015), -9.8 ± 34.1° and $-8.3°$ $\pm$ 39.0° (using
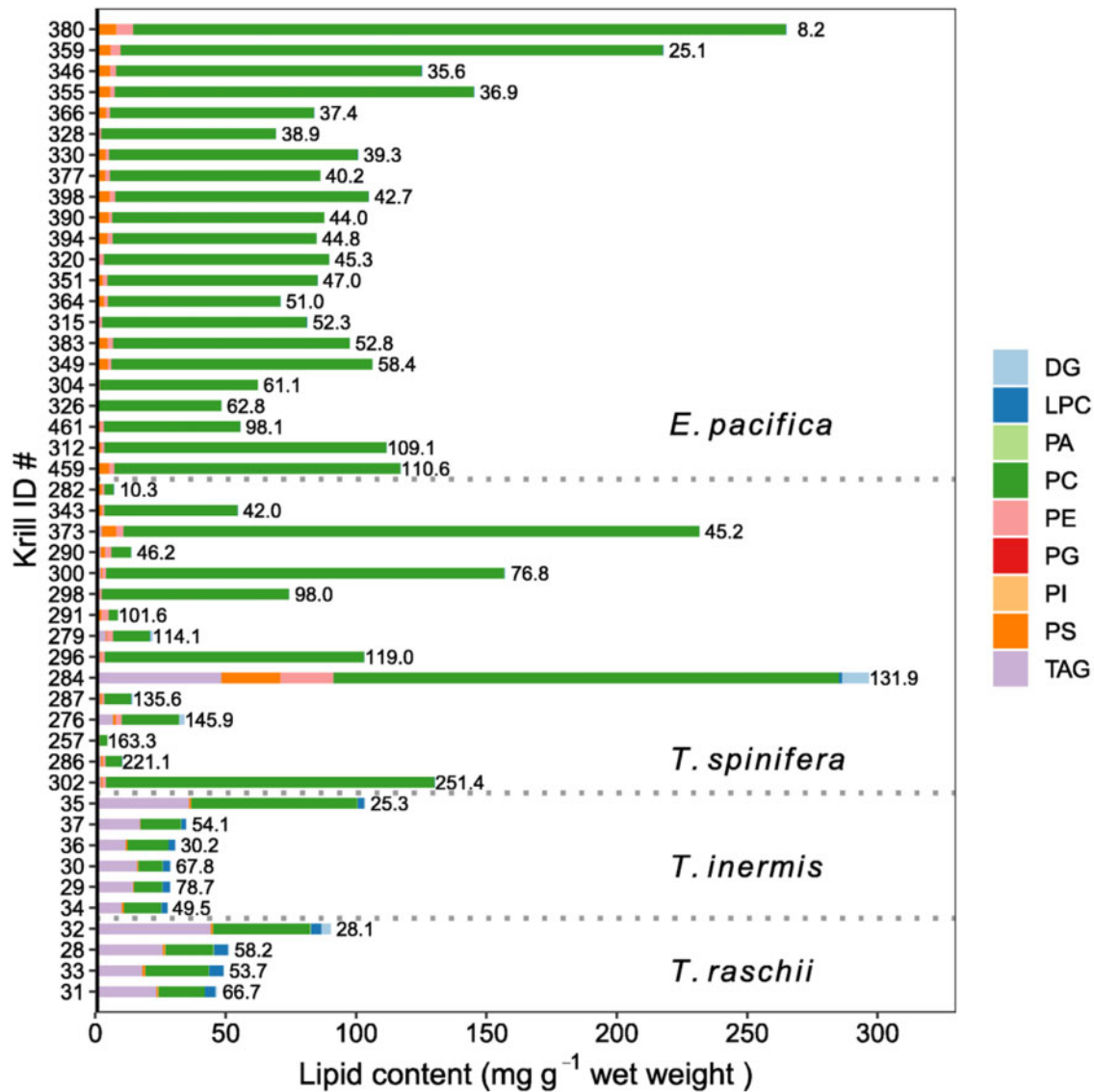
Figure 6. Summed concentrations of intact lipid classes determined in individual animals across the four species of krill evaluated in this study. Polar lipids as phospholipids (largely PC) were the dominant lipid class present in most species with significant TAG also observed in *Thysanoessa inermis* and *T. raschii*. Values to the right of each bar represent the mass (mg) of each respective krill. Other measured lipids include diglycerides (DG), LPC, phosphaitidic acid (PA), PC, phosphatidylgycerol (PG), phosphoatidylinositol (PI), phosphatidylserine (PS), TAG, and phosphatidylethanolamine (PE).

a similar stereo camera system as our study, although it was equipped with white lights and was only deployed at night; Levine *et al.,* 2018). The choice of which statistical distribution to represent *in situ* orientation had a relatively small effect where θ_{animal} was $2 \pm 31°$ using the mean and SD when not assuming a circular or wrapped distribution (i.e. f_{vM}). Although mean estimates for simulated mean θ_{animal} drawn from $N(2°, 31°)$ and $f_{\text{vM}}(1, 4.0)$ were all statistically similar, the von Mises distribution decreased the s.e. estimate (s.e. = 0.244) by a factor of four.

How sensitive are TS models to measured variability of parameter inputs?

Precision estimates (i.e. CV_{SE}) for modelled TS based on empirically measured parameter inputs ($n = 10\,000$) were all small at 38 (2.3%), 70 (2.1%), 120 (2.0%), and 200 kHz (1.9%). These corresponded larger integrated uncertainties (i.e. CV) of 230, 210, 200, and 190% where the SDs approximately doubled mean f_{bs}, which indicated large uncertainties in TS. Comparatively, the SDWBA reduced CV estimates by 3 and 1% at 120 and 200 kHz, respectively. Conversely, CV estimates at 38 and 70 kHz increased by 13 and 1%, respectively. Sample size intuitively had an effect on precision where mean CV_{SE} estimates increased by 89–90% and 67–68% for only 100 and 1000 simulations, respectively, which corresponds to mean modelled TS stabilizing after a few thousand simulations. The model was most sensitive to material properties at 110 kHz, while sensitivity to θ_{model} monotonically increased (Figure 9). Body shape also had an effect with respect to the large impulses in sensitivity, which both diverged from the sensitivities observed when
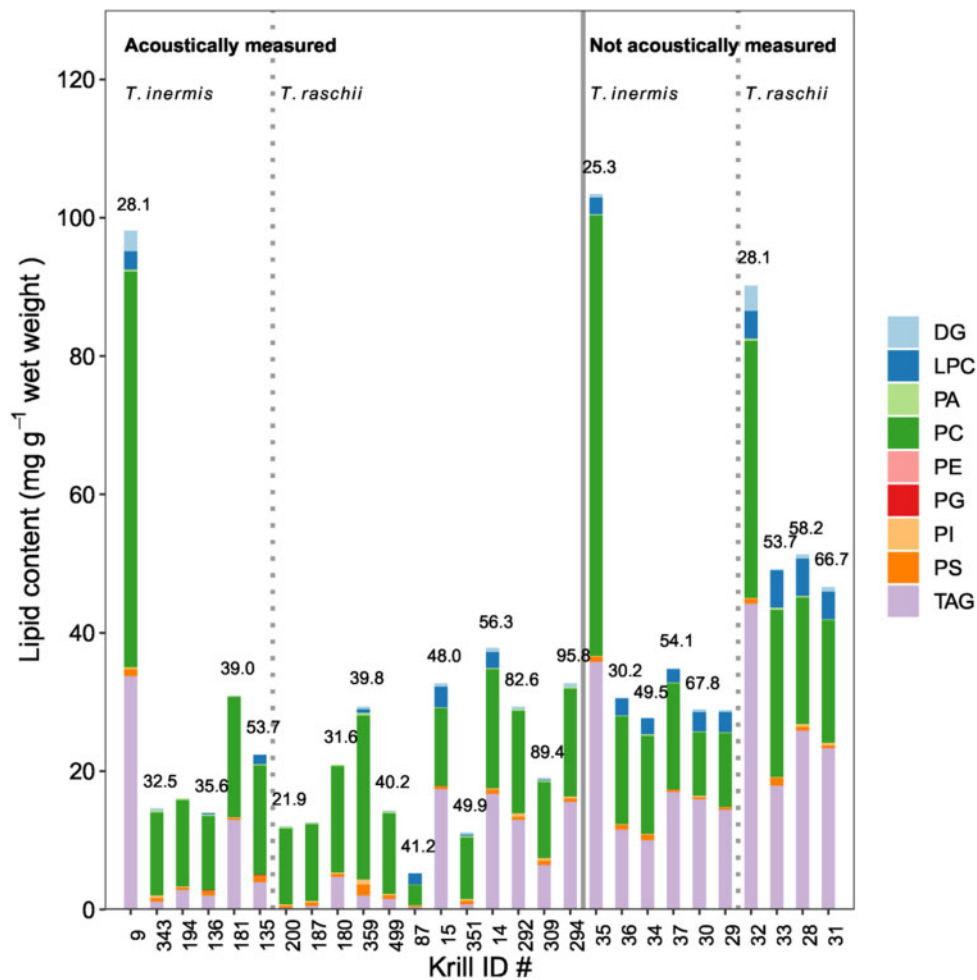
Figure 7. Comparisons of summed lipid classes in manipulated animals that underwent experimental acoustic experiments vs. pristine animals collected in parallel. Total lipid content varied between the two groups with differences in lipid class distributions observed. Pristine krill in particular showed elevated amounts of LPC indicative of fatty acid metabolism.
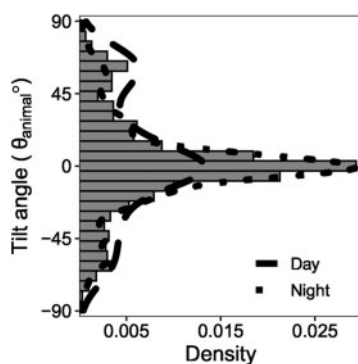

Figure 8. Most krill [mean: $1 \pm 31°$, f_{vM} ($\mu = 1.4$, $\kappa = 4.0$)] during both day and night were observed close to horizontal orientations (i.e. parallel to the sea surface). Distributions of krill orientations during the day (dashed, $n = 400$) and night (dotted, $n = 2300$) were significantly different ($D = 0.144$, $p < 0.01$), despite mean orientations being similar between day ($5° \pm 39°$) and night ($0° \pm 28°$).

using both the McGehee *et al.* (1998) and Smith *et al.* (2013) body shapes. RS in M was largely driven by the relationship between h and θ_{model}, which cooccur through the DWBA model.

The "simple" tapered shape from Smith *et al.* (2013) was particularly susceptible to very deep nulls. The absolute variability (i.e. extent of the 80% confidence intervals) in the RS of all parameters increased with frequency.

Variability due to M did not contribute to any frequency-dependent effect; however, the M distribution was much more constrained than the other parameters. When converted to biomass, the simulated mean and *SD* of M (0.098 ± 0.033, $n = 10\,000$) translates to a 4-fold change in biomass (i.e., from $M = 0.065–0.131$). Relative to this study's overall mean M, estimates reported in the literature typically shifted TS by up to a 6 dB, which also translates to approximately a 4-fold change in acoustic biomass (Table 2) compared to EBS/GOA measurements (Table 3). Large uncertainties can result from substantially smaller mean M estimates, which generate abnormally large biomass estimates that can skew the resulting distributions such as from Smith *et al.* (2010).

Discussion

Uncertainty in acoustic estimates of krill density, abundance, and biomass are generally larger than those from traditional sampling methods like net tows (Coyle and Pinchuk, 2002) and can be
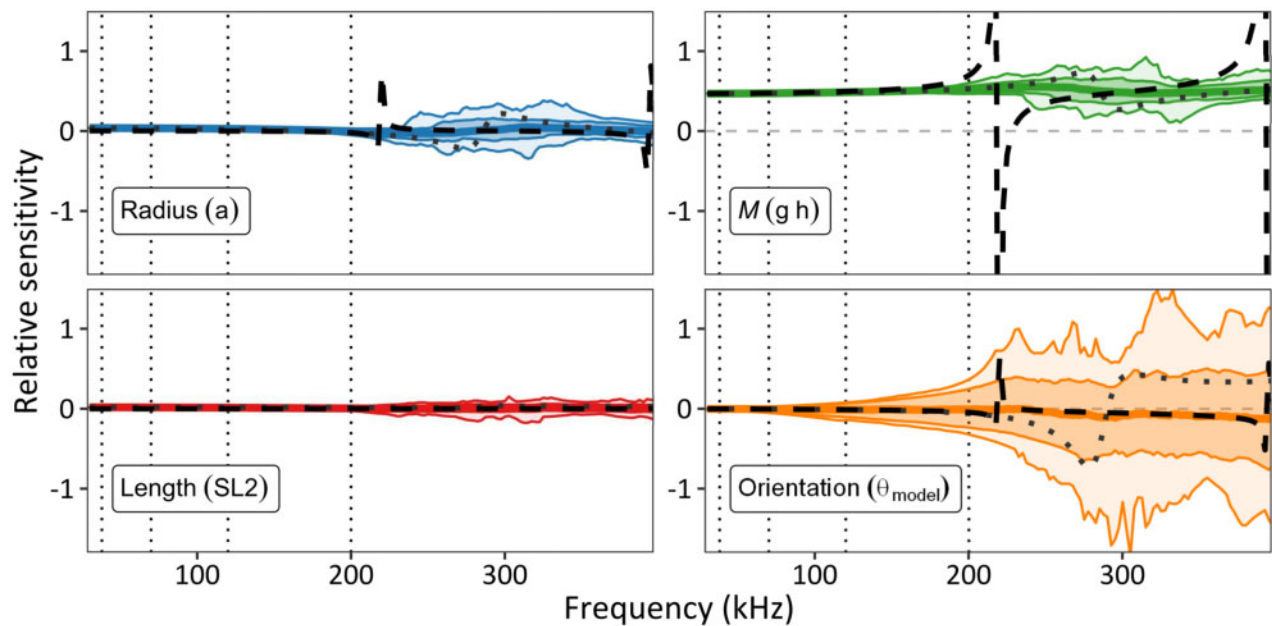
Figure 9. Frequency-dependent sensitivity to each tested parameter (radius, length, *M*, and θ_{model}) using scaled gradients calculated via automatic differentiation (coloured lines) show that the f_{bs} is uniformly sensitive to *M* across all frequencies until ~ 200 kHz while RS to orientation and radius increases with frequency. Spikes in RS at higher frequencies (e.g. 220 kHz) corresponded with null frequencies that were particularly affected by small changes in radius, orientation, and *M*. There was relatively strong agreement in median sensitivity among body shapes from this study, for generic *Euphausia superba* (McGehee *et al.*, 1998; grey dotted line), and generic tapered cylinder (Smith *et al.*, 2013; black dashed line) for all parameters except at particularly sensitive regions around 220 and 400 kHz. The 80% (dark shaded) and 95% (lightly shaded) confidence intervals expanded with increasing frequency. Vertical dashed lines represent 38, 70, 120, and 200 kHz. Each input was parameterized using empirical distributions of length (mm), $N(\mu = 17.9,\ \sigma = 11.6)$; maximum radius (mm), $N(2.2,\ 1.0)$; θ_{model} (radians), $N(1.59,\ 0.55)$; and *M*, $N(0.097,\ 0.001)$.

conceptually thought of as the upper limit on uncertainty estimates for abundance and biomass extrapolations (Warren and Wiebe, 2008). These uncertainties can further propagate into fishery and ecosystem models that rely on acoustic data to provide management recommendations (Hewitt and Demer, 1996; Ressler *et al.*, 2012). Consequently, improving scattering model output through more accurate estimates acoustic properties is crucial for providing more precise interpretations of acoustic backscatter data; however, measuring *in situ* distributions for each model parameter can be non-trivial and subject to numerous sampling biases (Simmonds and Maclennan, 2005). Parameter measurements for both GOA and EBS krill not only provide updated scattering models for sub-Arctic krill but also suggest that using distributions of model parameters rather than single values are necessary for generating more robust distributions of TS and evaluating how uncertainty propagates from each parameter to acoustic biomass.

Animal morphometry

Mean GOA lengths (Figure 3 and Table 1) were similar to measurements collected from four surveys between 2003 and 2013 (18.9 ± 2.2 mm; Simonsen *et al.*, 2016; Ressler, **unpublished data**); however, these surveys were dominated by *T. inermis*, *T. spinifera*, and *E. pacifica*, while material property measurements for GOA krill in this study comprised primarily *T. spinifera* and *E. pacifica*. Mean EBS lengths (16.4 ± 2.1 mm) were slightly smaller, but still similar, to those collected from net tows between 2004 and 2016 (18.6 ± 2.1 mm) whereby *T. raschii*

and *T. inermis* dominated in- and offshore species compositions, respectively (Smith, 1991; Coyle and Pinchuk, 2002; Ressler *et al.*, 2012, **unpublished** data), although the relative proportion of *T. spinifera* was higher than previous years.

Conversely, krill were approximately two-thirds the length of Antarctic *E. superba* used in other TS modelling studies (e.g. McGehee *et al.*, 1998). Since measurements from McGehee *et al.* (1998) were made on starved individuals, the assumption of a 40% increase in body girth (Demer and Conti, 2003) results in a proportionally similar difference between the maximum radius of *E. superba* and the sub-Arctic krill used in this study (Figure 4). Moreover, maximum carapace radius and both height in both EBS and GOA species were similar to those reported in Becker and Warren (2014). Although species-specific shapes were measured, other factors that could influence shape such as sexual dimorphism (Amakasu *et al.*, 2011) and reproductive status (Conti and Demer, 2006; Forman and Warren, 2010) were not directly measured and may account for some of the unexplained variation in the log-linear length–mass regressions.

Does lipid content, fluorescence, or length affect krill density?

This study found significant but weak linear relationships between *g* and body length for EBS *Thysanoessa* spp. similar to those reported in Smith *et al.* (2010) but not with results reported by Kristensen and Dalen (1986) for *Thysanoessa* spp. and Chu and Wiebe (2005) for *E. superba*. When scaled to SL1 length, our *g*-length regressions retain weak negative slopes for the overall

Table 2. Relative to the M (0.098 ± 0.033) measured in this study based on mean g (1.019 ± 0.010) and h (1.032 ± 0.015), estimates specific to the EBS and GOA from this study and those reported in the literature from the NWA, NEA, NEP, and ANT can generate large changes in TS at 120 kHz.

Location	Species	g	h	M	ΔTS (dB re: 1 m2) (120 kHz)	Biomass ratio
EBS/GOA[a]	*Euphausia pacifica* *Thysannoessa spinifera* *T. inermis* *T. raschii*	1.019 ± 0.010	1.032 ± 0.015	0.098 ± 0.033	–	–
EBS[b]	*T. spinifera* *T. inermis* *T. raschii*	1.018 ± 0.009	1.006 ± 0.008	0.055 ± 0.020	−5.9 ± 3.9	3.9× ± 2.5×
EBS[c]	*T. spinifera* *T. inermis* *T. raschii*	1.018 ± 0.006	1.022 ± 0.018	0.084 ± 0.029	−1.9 ± 3.4	1.6× ± 2.2×
ANT[d]	*E. superba*	1.024 ± 0.008	1.031 ± 0.008	0.106 ± 0.022	0.5 ± 0.6	−1.1× ± 1.2×
NWA[e]	*T. raschii*	1.013–1.018	1.032–1.046	0.103 ± 0.008	0.5 ± 1.8	−1.1× ± 1.5×
GOA[c]	*E. pacifica* *T. spinifera* *T. inermis*	1.021 ± 0.006	1.037 ± 0.011	0.110 ± 0.022	0.8 ± 1.9	−1.2× ± 1.5×
ANT[f]	*E. superba*	1.036 ± 0.007	1.028 ± 0.002	0.124 ± 0.014	1.9 ± 1.0	−1.5× ± 1.3×
NEP[g]	*Thysanoessa* spp.	1.058 ± 0.009	1.019 ± 0.009	0.151 ± 0.025	3.4 ± 1.4	−2.2× ± 1.4×
NEA[h]	*T. inermis* *T. raschii*	1.052–1.074	1.026 ± 0.005	0.173 ± 0.016	4.6 ± 0.7	−2.9× ± 1.2×

Positive and negative factors in the change of biomass indicate an increase or decrease, respectively. Values for g and h represent either the mean ± 1 SD or the minimum and maximum values depending on how material properties were reported for each study. Estimates of M represent the mean ± 1 SD based on the simulated distributions using g and h distributions from their respective studies. ΔTS indicate the mean ± 1 SD changes relative to the benchmark in the first row, which was the mean EBS/GOA M, and directly corresponds to changes in estimated biomass (i.e. Biomass ratio). Comparisons were made based on TS values rounded to the nearest 0.1 dB.
[a]Average of all data in this study.
[b]Smith *et al.* (2010).
[c]Region-specific estimates from this study.
[d]Chu and Wiebe (2005).
[e]Greenlaw and Johnson (1982).
[f]Foote (1990).
[g]Becker and Warren (2014).
[h]Køgeler *et al.* (1987).

Table 3. Summary of model parameters distributions measured for each species and region.

	EBS			GOA			EBS and GOA
	Length (mm)	g	h	Length (mm)	g	h	θ_{model}
Thysanoessa spinifera	16.5 ± 2.0	1.018 ± 0.006	1.022 ± 0.018	22.3 ± 4.9	1.021 ± 0.005	1.037 ± 0.011	1° ± 31°
T. inermis	15.8 ± 2.0	1.013 ± 0.005		11.4 ± 1.1	1.023 ± 0.003		
T. raschii	16.9 ± 2.2	1.018 ± 0.005		N/A	N/A		
Euphausia pacifica	N/A	N/A		18.6 ± 2.7	1.021 ± 0.006		

Distributions are represented by the mean ± 1 SD.

sample and GOA *T. spinifera* and *E. pacifica*. In context of g, these differences result in up to a ∼2.6% decrease (this study), 1% increase (Chu and Wiebe, 2005), and <0.1% increase (Kristensen and Dalen, 1986) for krill ranging from 10 to 30 mm. Although significant, it is important to interpret these results with caution due to most of the variability in g being explained by species and region (i.e. R_{C}^2; Figure 5), with TLE, length, mass, and fluorescence accounting for very little (i.e. R_{M}^2). Some lipids, such as relatively dense phospholipids (Hadley, 1985) and related classes, have been shown in other studies to impact overall buoyancy of

crustaceans (e.g. Campbell and Dower, 2003), but the lack of relationship between g and both chl_a fluorescence and lipid composition here suggests that other factors may also be at play (e.g. chlorophyll is not a complete proxy for food availability for these species; Falk-Petersen *et al.*, 2000) and requires further investigation. There was a significant difference in TLE and changes in lipid class composition between pristine and acoustically measured krill, which may indicate that physically handling krill before and/or after death may introduce error into lipid measurements; however, sample sizes for each comparison group

(i.e. same species from the same year) were extremely limited and this observation requires further investigation (Figure 7). Future experiments should be cautious about how animals are handled during acoustic measurements, preserved, and transported since all of these factors can potentially impact comparisons of lipid composition among species and relating this to *g*, or other acoustic properties.

Both the overall and region-specific mean *h* were substantially larger than previous measurements for EBS *Thysanoessa* spp. (Smith et al., 2010), but not northeast Atlantic *T. inermis* and *T. raschii* (Køgeler et al., 1987) and northeast Pacific *T. raschii* (Greenlaw and Johnson, 1982). Sound speed contrasts were also similar to those reported by Foote (1990) and Chu and Wiebe (2005) for Antarctic *E. superba*, which suggests that *h* estimates may be more generalizable than *g*. It is important to note that *h* was calculated for each region and not by species because bulk measurements were performed on a mix of different species, so EBS and GOA values may not accurately represent inter-animal and -species variability.

How does *in situ* orientation of krill vary?

In situ orientation of krill observed in this study show relatively strong agreement with literature reported values (most of which are of *E. superba*; Kils, 1981; Kristensen and Dalen, 1986; Endo, 1993; Kubilius et al., 2015; Levine et al., 2018), especially both mean and SDs (Figure 8). This also helps validate previous assumptions used in other modelling work for Alaskan sub-Arctic krill (Ressler et al., 2012; Smith et al., 2013). This demonstrates the strength of using optical systems to supplement acoustic measurements (Ryan et al., 2009) by not only providing *in situ* orientation information (e.g. Levine et al., 2018) but also other behaviours such as net size selection and swarming. Some of these behaviours can also be inferred based on diel differences in orientation distributions (Kristensen and Dalen, 1986; Simard and Sourisseau, 2009), although the difference between day- and night-time orientation distributions in this study were not very large. Generally, the assumption used in prior North Pacific krill surveys (Ressler et al., 2012) of a mean orientation close to horizontal relative to the sea surface and a wide SD is supported, although there was a large proportion of day-time orientations around ±45–60° that was not observed at night. Future day-time stereo camera measurements would be necessary to determine whether this distribution is valid for daytime krill behaviour, which could impact how acoustic backscatter data processed between day and night.

The relatively small difference in mean θ_{animal} simulated from von Mises and normal distributions was likely due to the relative concentration ($\kappa \approx 4$) around broadside incidence (i.e. $\theta_{animal} = 0°$). This was consistent with the normal distributions reported by Lawson et al. (2006), N ($\mu = 9.7°$, $\sigma = 59.3°$), Levine et al. (2018), N ($\mu = -8.3°$, $\sigma = 31°$), and their analogous von Mises distributions, f_{vM} ($\mu = -8.3°$, $\kappa = 2.8$), where mean θ_{animal} did not significantly change while variance substantially decreased. Therefore, the von Mises distribution provides an alternative approach to simulating θ_{animal} that produces more precise estimates that are directly compatible with both the bounds of *in situ* measurements, [$-90°$, $90°$], and converted θ_{model}, [$0°$, $180°$], for SDWBA parameterization.

How sensitive are TS models to measured variability of parameter inputs?

Generally, modelled TS is sensitive to parameter accuracy and variability. For example, TS appears to be sensitive to changes in orientation at higher frequencies regardless of body shape (Figure 9) due to steep decreases in TS as krill orientations moves away from broadside incidence (McGehee et al., 1998; Smith et al., 2013). The SDWBA provided fairly modest improvements to reducing model bias at 120 and 200 kHz, which suggests that uncertainty in σ_{ts} (or TS) was being driven more by some combination of the other model inputs. This could also suggest that the SDWBA (i.e. φ) may have been insufficiently parameterized and did not adequately mitigate the effect of off-broadside orientations. We note that the relatively large *CV* of simulated TS ($\sim$200% at 38, 70, 120, and 200 kHz) likely overestimates the expected uncertainty in *in situ* TS. Larger and more statistically robust distributions for length and model inputs would improve uncertainty in *in situ* TS by reducing the joint variability of model inputs. This was supported by the sharp decrease in the relative standard error (i.e. CV_{SE}) in modelled TS whereby our simulation demonstrated mean TS converged on the order of thousands simulations. The combination of both CV_{SE} and *CV* can help constrain an appropriate mean TS and general *in situ* uncertainty, respectively. For some parameters, sensitivity varied by frequency: mean TS at 38 and 70 kHz were nearly twice as sensitive to changes in body length and radius than at 200 kHz due to a shift where the transition from Rayleigh to geometric scattering occurs. However, uncertainty in sensitivity to length, radius, and *M* increased at frequencies greater than 200 kHz, resulting in some animals being sensitive to the combination of shape variability and orientation like shapes considered in Smith et al. (2013) and McGehee et al. (1998). This divergence could be due to differences in the length-to-radius ratio (e.g. 20.0 and 10.4 for the McGehee et al., 1998, and this study's shape, respectively) or other body shape features such as the longitudinal extent of the carapace. Conversely, median sensitivity to *M* was approximately uniform across all frequencies, with some exceptions such as spikes in sensitivity to *M* appeared to cooccur with those for orientation. Consequently, it is necessary to account for the relative precision and variability of each parameter at given frequencies to better assess model uncertainty.

RS to variability *M* highlights how error-prone TS estimates can be when *M* is parameterized either by using a single value rather than a distribution, or using literature values for other non-local species (Table 2). Measured variability in *M* corresponded to a change in mean TS by up to 5.2 dB or approximately a 3-fold change in biomass. Compared to this study, mean *M* estimates from other sub-Arctic krill measurements values increase TS by up to 4.6 ± 0.7 dB (Køgeler et al., 1987) or decrease by −5.9 ± 3.9 dB (Smith et al., 2010), which demonstrates that caution should be applied when using literature values for similar species. Previous Alaskan krill models applied *M* estimates of 0.030, 0.043, and 0.057 for low, medium, and high TS scenarios, respectively (Ressler et al., 2012) in biomass estimates for the EBS. These biomass estimates decreased by almost one order of magnitude when $M = 0.098$, which is a higher value driven mainly by a higher *h* estimate (Table 2).

TS modelling recommendations

Appropriate scattering model parameterization is an important consideration for survey design. It is important to draw input parameters from robust distributions that best represent target krill to help improve estimates of uncertainty. Some parameters can be obtained at sea from net sampled individuals (i.e. shape,

length) and material properties ([Chu and Wiebe, 2005](#); [Smith et al., 2010](#); [Smith et al., 2013](#)); however, while g can be measured for individuals, h represents bulk measurements of groups of animals and may therefore not precisely reflect an individual's true sound speed contrast. Moreover, *in situ* animal orientation is difficult to measure yet can have a significant effect on TS at frequencies typically used in fisheries acoustic surveys. Scattering model sensitivity to other potential variables such as *in situ* animal curvature/flexure, heterogeneous material properties, reproductive status, and ontogeny, have largely been understudied across all ecosystems and should be investigated further. For instance, [Amakasu et al. (2011)](#) demonstrated that sexual dimorphism and maturity stage strongly influences body shape and should be considered with respect to TS modelling. Regardless, measured parameters in this study ([Table 3](#)) highlight the importance of using local and region-specific parameter values whenever possible, cautiously drawing from broader distributions for parameters that may need to be generalized and assessing model sensitivity to try and adequately reflect how uncertainty in the parameter space propagates to estimates of TS.

While the parameter measurements made in this study inform future Alaska sub-Arctic krill surveys, both the species- and region-specific distributions can be used to help benchmark general krill TS modelling elsewhere and provide a framework for survey design. Correctly accounting for variability in TS model parameters in observed krill aggregations is essential to producing accurate survey estimates.

Acknowledgements

Data availability

The data underlying this article will be shared on reasonable request to the corresponding author.

References

Agostinelli, C., and Lund, U. 2017. R package 'circular': Circular statistics (version 0.4-93). https://r-forge.r-project.org/projects/circular (last accessed 15 September 2020).

Amakasu, K., Ono, A., Moteki, M., and Ishimaru, T. 2011. Sexual dimorphism in body shape of Antarctic krill (*Euphausia superba*) and its influence on target strength. Polar Science, 5: 179–186.

Amante, C., and Eakins, B. W. 2009. ETOPO1 1 arc-minute global relief model: procedures, data sources, and analysis. NOAA Technical Memorandum NESDIS NGDC-24. 19 pp.

Aydin, K., and Mueter, F. 2007. The Bering Sea: a dynamic food web perspective. Deep-Sea Research Part II: Topical Studies in Oceanography, 54: 2501–2525.

Bates, D., Mächler, M., Bolker, B., and Walker, S. 2015. Fitting linear-mixed effects models using lme4. Journal of Statistical Software, 67: 48.

Baydin, A. G., Pearlmutter, B. A., Radul, A. A., and Siskind, J. M. 2018. Automatic differentiation in machine learning: a survey. Journal of Machine Learning Research, 18: 1–43.

Becker, K. N., and Warren, J. D. 2014. Material properties of Northeast Pacific zooplankton. ICES Journal of Marine Science, 71: 2550–2563.

Bestley, S., Raymon, B., Gales, N. J., Harcourt, R. G., Hindell, M. A., Jonsen, I. D., Nicol, S., et al. 2017. Predicting krill swarm characteristics important for marine predators foraging off East Antarctic. Ecography, 41: 996–1012.

Bird, S., Marur, V. R., Sniatynski, M. J., Greenberg, H. K., and Kristal, B. S. 2011. Lipidomics profiling by high-resolution LC-MS and high-energy collisional dissociation fragmentation: focus on characterization of mitochondrial cardilipins and monolysocardiolipins. Analytical Chemistry, 83: 940–949.

Buckley, T. W., Ortiz, I., Kotwicki, S., and Aydin, K. 2016. Summer diet composition of walleye pollock and predator-prey relationships with copepods and euphausiids in the eastern Bering Sea, 1987–2011. Deep-Sea Research Part II: Topical Studies in Oceanography, 134: 302–311.

Cabrol, J., Trombetta, T., Amaudrut, S., Aulanier, F., Sage, R., Tremblay, R., Nozais, C., et al. 2019. Trophic niche partitioning of domination North-Atlantic krill species. *Meganyctiphanes norvegica*, *Thysanoessa inermis*, and *T. raschii*. Limnology and Oceanography, 64: 156–181.

Campbell, R. W., and Dower, J. F. 2003. Role of lipids in the maintenance of neutral buoyancy by zooplankton. Marine Ecology Progress Series, 263: 93–99.

Chu, D., Foote, K. G., and Stanton, T. K. 1993. Further analysis of target strength measurements of Antarctic krill at 38 and 120 kHz: comparison with deformed cylinder model and inference of orientation distribution. The Journal of the Acoustical Society of America, 93: 2985–2988.

Chu, D., and Wiebe, P. H. 2005. Measurements of sound-speed and density contrasts of zooplankton in Antarctic waters. ICES Journal of Marine Science, 62: 818–831.

Conti, S. G., and Demer, D. A. 2006. Improved parameterization of the SDWBA for estimating krill target strength. ICES Journal of Marine Science, 63: 928–935.

Coyle, K. O., and Pinchuk, A. I. 2002. The abundance and distribution of euphausiids and zero-age pollock on the inner shelf of the southeast Bering Sea near the Inner Front in 1997–1999. Deep-Sea Research Part II: Topical Studies in Oceanography, 49: 6009–6030.

Demer, D. A., and Conti, S. G. 2003. Reconciling theoretical versus empirical target strengths of krill: effects of phase variability on the distorted-wave Born approximation. ICES Journal of Marine Science, 60: 429–434.

Endo, Y. 1993. Orientation of Antarctic krill in an aquarium. Nippon Suisan Gakkaishi, 59: 465–468.

Falk-Petersen, S., Hagen, W., Kattner, G., Clarke, A., and Sargent, J. 2000. Lipids, trophic relationships, and biodiversity in Arctic and Antarctic krill. Canadian Journal of Fisheries and Aquatic Sciences, 57: 178–191.

Farley, E. V., Jr., Heintz, R. A., Andrews, A. G., and Hurst, T. P. 2016. Size, diet, and condition of age-0 Pacific cod (*Gadus macrocephalus*) during warm and cool climate states in the eastern Bering Sea. Deep Sea Research Part II: Topical Studies in Oceanography, 134: 247–254.

Foote, K. G. 1990. Speed of sound in *Euphausia superba*. The Journal of the Acoustical Society of America, 87: 1405–1408.

Forman, K. A., and Warren, J. D. 2010. Variability in the density and sound-speed of coastal zooplankton and nekton. ICES Journal of Marine Science, 67: 10–18.

Fox, J., and Weisberg, S. 2019. An R Companion to Applied Regression, 3rd edn. Sage, Thousand Oaks, CA.

Greenlaw, C. F., and Johnson, R. K. 1982. Physical and acoustical properties of zooplankton. The Journal of the Acoustical Society of America, 72: 1706–1710.

Hadley, N. F. 1985. The Adaptive Role of Lipids in Biological Systems. John Wiley & Sons, New York, NY.

Hamner, W. M., Hamner, P. P., Strand, S. W., and Gilmer, R. W. 1983. Behavior of Antarctic krill, *Euphausia superba*: chemoreception, feeding, schooling, and molting. Science, 220: 433–435.

Harvey, H. R., Pleuthner, R. L., Lessard, E. J., Bernhardt, M. J., and Tracy Shaw, C. 2012. Physical and biochemical properties of euphausiids *Thysanoessa inermis*. *Thysanoessa raschii*, and *Thysanoessa longipes in the eastern Bering Sea*. Deep-Sea Research Part II: Topical Studies in Oceanography, 65–70: 173–183.

Hewitt, R. P., and Demer, D. A. 1996. Lateral target strength of Antarctic krill. ICES Journal of Marine Science, 53: 297–302.

Holliday, D. V. 1977. Extracting bio-physical information from the acoustic signature of marine organisms. *In* Oceanic Sound Scattering Prediction, pp. 619–624. Ed. by N. R. Andersen and B. J. Zahuranec. Plenum, New York, NY.

Honkalehto, T., Jones, D., McCarthy, A., McKelvey, D., Guttormsen, M., Williams, K., and Williamson, N. 2009. Results of the echo integration-trawl survey of walleye pollock (*Theragra chalcogramma*) on the U.S. and Russian Bering Sea shelf in June and July 2008. U.S. Department of Commerce, NOAA Technical. Memorandum NMFS-AFSC-194. 56 pp. https://www.afsc.nooa.gov/Publications/AFSC-TM/NOAA-TM-AFSC-194.pdf

Honkalehto, T., McCarthy, A., and Lauffenburger, N. 2018. Results of the acoustic-trawl survey of walleye pollock (Gadus chalcogrammus) on the U.S. Bering Sea shelf in June – August 2016 (DY1608). AFSC Processed Rep. 2018-03. 78 p. Alaska Fish. Sci. Cent., NOAA, Natl. Mar. Fish. Serv., 7600 Sand Point Way NE, Seattle WA 98115. http://www.afsc.noaa.gov/Publications/ProcRpt/PR2018-03.pdf

Hunt, G. L., Jr., Ressler, P. H., Gibson, G. A., De Robertis, A., Aydin, K., Sigler, M. F., Ortiz, I., *et al.* 2016. Euphausiids in the eastern Bering Sea: a synthesis of recent studies of euphausiid production, consumption, and population control. Deep Sea Research Part II: Topical Studies in Oceanography, 134: 204–222.

Jech, J. M., Horne, J. K., Chu, D., Demer, D. A., Francis, D. T. I., Gorska, N., Jones, B., *et al.* 2015. Comparisons among ten models of acoustic backscattering used in aquatic ecosystem research. The Journal of the Acoustical Society of America, 138: 3742–3764.

Jech, J. M., Lawson, G. L., and Lavery, A. C. 2017. Wideband (15-260 kHz) acoustic volume scattering spectra of Northern Krill (*Meganyctiphanes norvegica*) and butterfish (*Peprilus triacanthus*). ICES Journal of Marine Science, 74: 2249–2261.

Jones, B. A., Lavery, A. C., and Stanton, T. K. 2009. Use of distorted born wave approximation to predict scattering by inhomogeneous objects: application to squid. The Journal of the Acoustical Society of America, 125: 73–88.

Jones, E., Olphant, E., and Peterson, P. 2001. SciPy: open source scientific tools for Python. http://www.scipy.org (Last accessed 14 October 2019).

Jones, D. T., Lauffenburger, N., Williams, K., and De Robertis, A. 2019. Results of the acoustic-trawl survey of walleye pollock (*Gadus chalcogrammus*) in the Gulf of Alaska, June–August 2017 (DY2017-06). AFSC Processed Rep. 2019-08, 110 p. Alaska Fish. Sci. Cent., NOAA, Natl. Mar. Fish. Serv., 7600 Sand Point Way NE, Seattle WA 98115.

Kils, U. 1981. Swimming behavior, swimming performance, and energy balance of Antarctic krill, *Euphausia superba*. BIOMASS

Science Series, 3. Scott Polar Research Institute, Cambridge, UK. 122 pp.

Knutsen, T. W., Melle, W., and Calise, L. 2001. Determining the mass density of marine copepods and their eggs with a critical focus on some of the previously used methods. Journal of Plankton Research, 23: 859–873.

Køgeler, J. W., Falk-Petersen, S., Kristensen, Å., Pettersen, F., and Dalen, J. 1987. Density- and sound speed contrasts in sub-Arctic zooplankton. Polar Biology, 8: 231–235.

Kolber, Z., and Falkowski, P. G. 1993. Use of active fluorescence to estimate phytoplankton photosynthesis *in situ*. Limnology and Oceanography, 38: 1646–1665.

Kristensen, Å., and Dalen, J. 1986. Acoustic estimation of size distribution and abundance of zooplankton. The Journal of the Acoustical Society of America, 80: 601–611.

Kubilius, R., Ona, E., and Calise, L. 2015. Measuring *in situ* krill tilt orientation by stereo photogrammetry: examples for *Euphausia superba* and *Meganyctiphanse norvegica*. ICES Journal of Marine Science, 72: 2494–2505.

Landler, L., Ruxton, G. D., and Malkemper, E. P. 2018. Circular data in biology: advance for effectively implementing statistical procedures. Behavioral Ecology and Sociobiology, 72, 10.1007/s00265-020-02881-6.

Lawson, G. L., Wiebe, P. H., Ashjian, C. J., Chu, D., and Stanton, T. K. 2006. Improved parameterization of Antarctic krill target strength models. The Journal of the Acoustical Society of America, 119: 232–242.

Levine, M., Williams, K., and Ressler, P. H. 2018. Measuring the in situ tilt orientation of fish and zooplankton using stereo photogrammetric methods. Limnology and Oceanography: Methods, 16: 390–399.

Li, C. 2019. JuliaCall: an R package for seamless integration between R and Julia. The Journal of Open Source Software, 4: 1284.

Lucca, B. M. 2020. acousticTS: Scattering models for calculating acoustic target strength. https://www.github.com/brandynlucca/acousticTS (last accessed 1 February 2021).

Mauchline, J. 1980. Measurement of body length of *Euphausia superba* Dana. *In* BIOMASS Handbook. pp. 4–9. Scott Polar Research Insitute. Cambridge, UK.

McGehee, D. E., O'Driscoll, R. L., and Martin-Tray, L. V. 1998. Effects of orientation on acoustic scattering for Antarctic krill at 120 kHz. Deep-Sea Research Part II: Topical Studies in Oceanography, 45: 1273–1294.

McQuinn, I. H., Dion, M., and St Pierre, J. 2013. The acoustic multifrequency classification of two sympatric euphausiid species (*Meganyctiphanes norvgeica* and *Thysanoessa raschii*), with empirical and SDWBA model validation. ICES Journal of Marine Science, 70: 636–649.

Methot, R. D. 1986. Frame trawl for sampling pelagic juvenile fish. CALCOFI Rep. Vl XXVII, 267–278. CALCOFI. La Jolla, CA.

Nakagawa, S., and Schielzeth, H. 2013. A general and simple method for obtaining R^2 from generalized linear mixed-effects models. Methods in Ecology and Evolution, 4: 133–142.

Pante, E., and Simon-Bouhet, B. 2013. marmap: a package for importing, plotting, and analyzing bathymetric and topograhic data in R. PLoS One, 8: e73051.

Pleuthner, R. L., Shaw, C. T., Schatz, M. J., Lessard, E. J., and Harvey, H. R. 2016. Lipid markers of dietary history and their retention during experimental starvation in the Bering Sea euphausiid *Thysanoessa raschii*. Deep-Sea Research Part II: Topical Studies in Oceanography, 134: 190–203.

Python Software Foundation. 2018. Python language reference, version 3.7.1. Wilmington, DE. https://www.python.org (last accessed 14 October 2019).

R Core Team. 2020. R: A language and environment for statistical computing. R Foundation for Statistical Computing, Vienna, Austria. https://www.R-project.org/ (last accessed 6 July 2020).

Reiss, C. S., Cossio, A. M., Loeb, V., and Demer, D. A. 2008. Variations in the biomass of Antarctic krill (*Euphausia superba*) around the South Shetland Islands, 1996–2006. ICES Journal of Marine Science, 65: 497–508.

Ressler, P. H. Biennial contributions on acoustic indices of euphausiid ("krill") abundance in the eastern Bering Sea (contributed since 2011) and Gulf of Alaska (contributed since 2014). *In* Ecosystem Considerations Stock Assessment and Fishery Evaluation Reports. Ed. by S. Zador *et al.* https://archive.fisheries. noaa.gov/afsc/REFM/Stocks/assessments.htm (last accessed 3 March 2021).

Ressler, P. H., Robertis, A. D., Warren, J. D., Smith, J. N., and Kotwicki, S. 2012. Developing an acoustic survey of euphausiids to understand trophic interactions in the Bering Sea ecosystem. Deep-Sea Research Part II: Topical Studies in Oceanography, 65–70: 184–195.

Revels, J., Lubin, M., and Papamarkou, T. 2016. Forward-Mode automatic differentiation in Julia. Arxiv. https://arxiv.org/abs/1607. 07892.

Ryan, T. E., Kloser, R. J., and Macaulay, G. J. 2009. Measurement and visual verification of fish target strength using an acoustic-optical system attached to a trawlnet. ICES Journal of Marine Science, 66: 1238–1244.

Sakinan, S., Lawson, G. L., Wiebe, P. H., Chu, D., and Copley, N. J. 2019. Accounting for seasonal and composition-related variability in acoustic material properties in estimating copepod krill target strength. Limnology and Oceanography Methods, 17: 607–625.

Sameoto, D. D., Cochrane, N. A., and Herman, A. W. 1993. Convergence of acoustic, optical, and net-catch estimates of euphausiid abundance. The use of artificial light to reduce net avoidance. Canadian Journal of Fisheries and Aquatic Sciences, 50: 334–346.

Sameoto, D. D., Harris, R., Wiebe, P. H., Runge, J., Postel, L., Dunn, J., Miller, C., and Coombds, S. 2000. Collecting zooplankton. *In* ICES Zooplankton Methodology Manual. pp. 55–81. Ed. by R. Harris, P. H. Wiebe, J. Lenz, H. Skjoldal and M. Huntley. Academic Press, London, UK. 684 pp.

Simard, Y., and Sourisseau, M. 2009. Diel changes in acoustic and catch estimates of krill biomass. ICES Journal of Marine Science, 66: 1318–1325.

Simmonds, E., and Maclennan, D. 2005. Fisheries Acoustics: Theory and Practice, 2nd ed. Blackwell, Oxford.

Simonsen, K. A., Ressler, P. H., Rooper, C. N., and Zador, S. G. 2016. Spatio-temporal distribution of euphausiids: an important component to understanding ecosystem processes in the Gulf of Alaska and eastern Bering Sea. ICES Journal of Marine Science, 73: 2020–2036.

Smith, S. L. 1991. Growth, development, and distribution of euphausiids *Thysanoessa raschii* (M. Sars) and *Thysanoessa inermis* (Krøyer) in the southeastern Bering Sea. Polar Research, 10: 461–478.

Smith, J. N., Ressler, P. H., and Warren, J. D. 2010. Material properties of euphausiids and other zooplankton from the Bering Sea. The Journal of the Acoustical Society of America, 128: 2664–2680.

Smith, J. N., Ressler, P. H., and Warren, J. D. 2013. A distorted wave Born approximation target strength model for Bering Sea euphausiids. ICES Journal of Marine Science, 70: 204–214.

Soetaert, K., and Petzoldt, T. 2018. marelac: Tools for aquatic sciences. R package version 2.1.9. https://CRAN.R-project.org/pack age=marelac (last accessed 12 August 2019).

Stanton, T. K., Chu, D., and Wiebe, P. H. 1998. Sound scattering by several zooplankton groups. II. Scattering models. The Journal of the Acoustical Society of America, 103: 236–253.

Stanton, T. K., and Chu, D. 2000. Review and recommendations for the modelling of acoustic scattering by fluid-like elongated zooplankton: euphausiids and copepods. ICES Journal of Marine Science, 57: 793–807.

Warren, J. D., and Smith, J. N. 2007. Density and sound speed of two gelatinous zooplankton: ctenophore (*Mnemiopsis leidyi*) and lion's mane jellyfish (*Cyanea capillata*). The Journal of the Acoustical Society of America, 122: 574–580.

Warren, J. D., and Wiebe, P. H. 2008. Accounting for biological and physical sources of acoustic backscatter improves estimates of zooplankton biomass. Canadian Journal of Fisheries and Aquatic Sciences, 65: 1321–1333.

Wickham, H., Averick, M., Bryan, J., Chang, W., McGowan, L. D., François, R., Grolemund, G., *et al.* 2019. Welcome to the tidyverse. Journal of Open Source Software, 4: 1686.

Wiebe, P. H., Lawson, G. L., Lavery, A. C., Copley, N. J., Horgan, E., and Bradley, A. 2013. Improved agreement of net and acoustical methods for surveying euphausiids by mitigating avoidance using a net-based LED strobe light system. ICES Journal of Marine Science, 70: 650–664.

Williams, K., Towler, R., Goddard, P., Wilborn, R., and Rooper C., 2016. Sebastes stereo image analysis software. AFSC Processed Rep. 2016-03. 42 pp. Alaska Fish. Sci. Cent., NOAA, Natl. Mar. Fish. Serv., 7600 Sand Point Way NE, Seattle WA 98115. http:// www.afsc.noaa.gov/Publications/ProcRpt/PR2016-03.pdf

Yayanos, A. A., Benson, A. A., and Nevenzel, J. C. 1978. The pressure-volume-temperature (PVT) properties of lipid mixture from a marine copepod, *Calanus plumchrus*: implications for buoyancy and sound scattering. Deep Sea Research, 25: 257–268.

Handling editor: Roland Proud